ADVANCED FUNCTIONAL MATERIALS
www.afm-journal.de

M13 Bacteriophage as Materials for Amplified Surface Enhanced Raman Scattering Protein Sensing

*Ju Hun Lee, Phyllis F. Xu, Dylan W. Domaille, Chulmin Choi, Sungho Jin, and Jennifer N. Cha**

Because of their unique properties, nanomaterials have been actively investigated in recent years for biosensing applications. A typical approach for biomarker detection is to attach capture or detection antibodies to nanomaterials, allow the analyte to bind, and measure the resulting change in signal. While antibodies or aptamers possess at most one binding site each for the nanomaterial and analyte, it is shown that the high surface area filamentous M13 bacteriophage can be utilized as a scaffold for generating an amplified signal. Since only a few proteins at the tip of the micrometer-long virus are involved in antigen binding, the rest of the bacteriophage can be augmented with hundreds of functional groups, each of which can bind to a specific nanomaterial. It is demonstrated that the combination of DNA-modified M13 bacteriophage and surface enhanced Raman spectroscopy (SERS) active nanoparticles can be used to produce exponential gains in Raman signal compared to that of antibodies at the same antigen concentration. Because of these high sensitivities, Raman measurements can be made directly from individual silica microparticles, potentially enabling future single step identification and analysis of different proteins in complex mixtures, while avoiding additional processing steps or prepatterned microarrays.

1. Introduction

New diagnostics that can sense for particular biomarkers remain in critical need for early stage disease detection and prevention.[1–3] For biomedical applications, the naturally existing M13 bacteriophage has shown promising use as materials for therapy and sensing. The phage are resistant to elevated temperatures, high salt concentration, acidic pH, and chaotropic agents,[4,5] are non-toxic and do not initiate an immune response in humans.[6] Phage are also easily produced in *E. coli* and possess unique biochemical structural features that make them ideal candidates for chemical or genetic modification.[7–9] Because of these characteristics, M13 viruses have been used as drug delivery carriers,[10,11] scaffolds for in vitro and in vivo imaging,[4,12–14] and biosensors.[5,15–17] To this end, we have recently demonstrated that chemically modified DNA-M13 bacteriophage can be used as bioanalytical platforms that enable facile and rapid detection of antigens in solution.[18–20]

Among the many different detection modalities shown from nanomaterials,[1,2,21–29] sensing strategies based on surface enhanced Raman spectroscopy (SERS) has been a particularly promising approach. The Raman signal is greatly enhanced when molecules are brought near the surface of noble metals in a variety of morphologies; the largest effects are seen from plasmonic coupling arising from nanometer gap junctions.[30–39] In addition to being very sensitive, SERS can be used as a molecular fingerprinting technique due to the detailed spectrum consisting of narrow lines which allows resolution of spectral features for simultaneous detection of different probes and biomarkers.[33,40–43] This is in contrast to the more conventional ELISA based sensors where only one type of signal (e.g., colorimetric) is generated. Because SERS signals depend greatly on the distance between the molecule and the metal surface, control over the position of the nanoparticle and the Raman active dye is crucial for generating large, reproducible SERS signals.[44–47] To resolve problems arising from inconsistent enhancement factors and uncertainties in SERS signal, some research has focused on embedding Raman active dyes within the nanostructures.[44–47]

We report here a biosensor system that combines the use of DNA-conjugated SERS-active Au@Ag core–shell nanoparticles with DNA-modified M13 bacteriophage. By reacting DNA-conjugated M13 viruses with DNA-SERS particles, we demonstrate that high loadings of nanoparticles can be captured to a single phage that lead to exponential increases in Raman intensity much larger than what can be achieved with antibodies. While SERS has been used for detection previously, amplifying SERS

J. H. Lee, P. F. Xu, Prof. S. Jin, Prof. J. N. Cha
Department of Nanoengineering
and Materials Science and Engineering Program
University of California
San Diego, 9500 Gilman Dr. M/C 0448
La Jolla, CA, 92093-0448, USA
E-mail: Jennifer.Cha@Colorado.edu
Dr. D. W. Domaille, Prof. J. N. Cha
Department of Chemical and Biological Engineering
University of Colorado
Boulder, 596 UCB, Boulder, CO, 80303-1904, USA
Dr. C. Choi, Prof. S. Jin
Department of Mechanical Engineering
University of California
San Diego, 9500 Gilman Dr., M/C 0411,
La Jolla, CA, 92093-0411, USA

DOI: 10.1002/adfm.201303331

© 2013 WILEY-VCH Verlag GmbH & Co. KGaA, Weinheim

signals through specific biomolecular interactions and taking advantage of the large macromolecular structure of the antigen-binding agent have not been demonstrated.

2. Results and Discussion

In previous work, phage display panning yielded M13 bacteriophage that bound to the model antigen anti-goat rabbit immunoglobulin (IgG).[18] In subsequent work, we further reported the use of 1-ethyl-3-(3-dimethylaminopropyl)carbodiimide (EDC) and succinimidyl-3-(2-pyridyldithio)propionate (SPDP)/ sulfosuccinimidyl-4-(N-maleimido-methyl) cyclo-hexane-1-carboxylate (s-SMCC) for conjugating DNA oligonucleotides to the p8 major capsid proteins on the virus.[18,19] However, due to undesired intra- and inter-virus crosslinking and low DNA conjugation yields, aldehyde conjugated phage and hydrazine-terminated DNA was used instead. In doing so, we were able to take advantage of the high chemoselectivity of acyl hydrazone formation under mild conditions without considerably affecting the biological reactivity of the p3 proteins.[20,48] Benzaldehyde groups were first conjugated to phage by reacting the nucleophilic amines of the p8 proteins with 4-formyl succinimidyl benzoate. The aldehyde-derivatized M13 were then reacted with hydrazide-derivatized DNA in 100 mM NH_4OAc buffer, pH 4.8 for 24 h.[20] The DNA phage conjugates were characterized by densitometric analysis of SDS-PAGE gels after Coomassie staining (Figure S1, Supporting Information), which showed that 315 ± 41 DNA strands could be conjugated to the M13 bacteriophage (Supporting Information, S2).

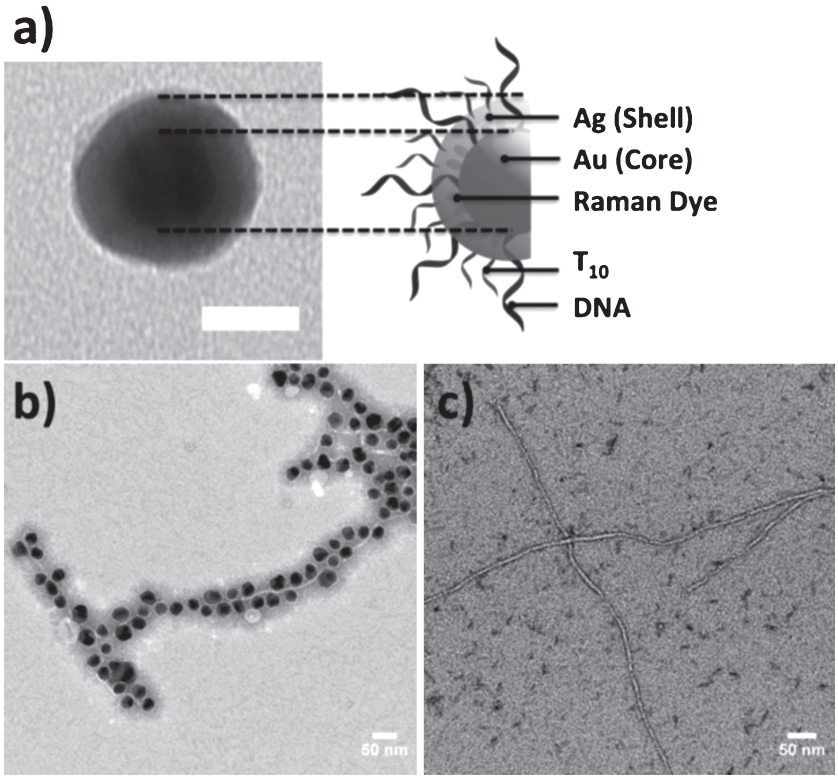

Figure 1. a) TEM image of T_{10} passivated DNA-Cy3-Au@Ag nanoparticles and nanoparticle schematic (Scale bar = 20 nm). b) Uranyl acetate stained TEM images of DNA conjugated phage after reaction with complementary DNA-Cy3-Au@Ag nanoparticles. c) Uranyl acetate stained TEM images of aldehyde conjugated phage after reaction with DNA-Cy3-Au@Ag nanoparticles.

Next, we attempted to bind SERS nanoparticles to the DNA-conjugated phage. In order to optimize the detection scheme, we first sought to produce DNA conjugated SERS nanocrystals that show large enhancement factor (EF) values. Recently, Lim et al. reported the synthesis of SERS active nanostructures with narrow distribution of EF values[45] by conjugating thiolated Cy3 labeled DNA to 20 nm gold nanoparticles (Au NPs). In order to increase the number of dyes per particle, we decided to alter the synthesis by directly conjugating the Raman-active molecules to the Au NPs first, followed by addition of thiolated DNA. For this, thiolated Cy3 was synthesized (Figure S3, Supporting Information) and then reacted with 20 nm Au NPs at 300:1 molar ratios of Cy3:Au NPs. Next, thiolated DNA was conjugated to the Cy3-AuNPs by salt aging.[49] To measure the number of bound Cy3, the nanoparticles were reacted with DTT to liberate the dye which was quantified by UV-Vis absorbance measurements. From this it was determined that the average number of Cy3 per particle was 225 ± 25 (n = 3). To produce SERS active nanoparticles, the DNA and Cy3 conjugated Au NPs were next reacted with poly(N-vinylpyrrolidone) (PVP), sodium L-ascorbate, and silver nitrate in 300 mM NaCl to form uniform silver shells around each Au NP (**Figure 1**a and Supporting Information, Figure S4).[44,50–53] The average thickness of the silver shells on the Au NPs was found to be 10 ± 2 nm (n = 50). The UV-Vis spectrum showed a plasmon band shift from ≈520 nm to ≈410 nm without any secondary surface plasmon resonance modes (Figure S4, Supporting Information), indicating that uniform silver shells were formed on the gold without any directional or asymmetric growth. To confirm that the DNA on the Au@Ag NPs was able to hybridize to complementary DNA, we performed control experiments with complementary and non-complementary 10 nm Au NPs (Figure S5, Supporting Information). The DNA-Cy3-Au@Ag only bound to Au NPs that were conjugated with complementary DNA, indicating that the DNA on the SERS particles showed specific base pairing. Furthermore, because the exposed silver surfaces were later found to induce nonspecific binding which is detrimental for biosensing, short DNA (T_{10}) strands were added to passivate the Au@Ag NPs through salt aging[54] (Figure S6, Supporting Information). In order to demonstrate that the extra T_{10} strands helped prevent nonspecific binding, we reacted the particles with BSA blocked silica microbeads. After one hour incubation and centrifugation, the color of the microbead pellet after reaction with non-passivated DNA-Au@Ag NPs was visibly darker than with the T_{10} passivated NPs (Figure S7a, Supporting Information). These observations also correlated with UV-Vis measurements

© 2013 WILEY-VCH Verlag GmbH & Co. KGaA, Weinheim

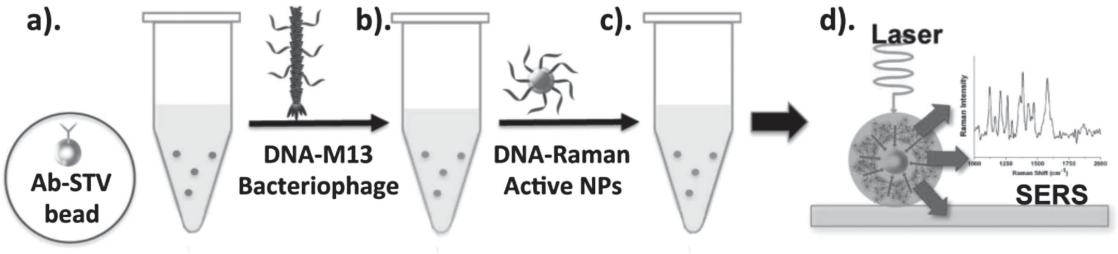

Scheme 1. Quantitative SERS sensing with DNA-phage: a) Antigen were first captured onto silica microbeads, b) DNA conjugated M13 bacteriophage were added next to the silica microbeads followed by c) DNA conjugated Raman active nanoparticles. d) Individual silica beads were measured by Raman spectroscopy.

which determined the amount of Au@Ag NPs in the supernatant (Figure S7b, Supporting Information).

Next, to determine the SERS response of the particles, we measured Raman intensity as a function of nanoparticle number. For this, an array of Si pillars 4 μm in diameter were photolithographically patterned to match the laser spot size of the micro-Raman. These micropatterned substrates were then made hydrophilic through UV-ozone treatment, and varying concentrations of the DNA-Cy3-Au@Ag nanoparticles were absorbed to the pillar arrays in 150 mM NaCl. After counting the number of nanoparticles on individual pillars in each sample by scanning electron microscopy (SEM), micro-Raman analysis was performed. For the Raman spectroscopy measurements, we measured the fingerprint peak region of Cy3 at 1580 cm^{-1} using laser excitations of 543.5 nm and 632.8 nm (He-Ne laser) (=130 μW, accumulation time: 30 s) (S8, Figure S9, Supporting Information). The SERS EF values were determined by normalizing the laser power (130 μW) and acquisition time for all samples measured. On the basis of these measurements, the calculated SERS EF were determined to be 1.39×10^6 and 1.29×10^5 with 543.5 nm and 632.8 nm excitation respectively (S10, Supporting Information).

In order to determine if the DNA-Cy3-Au@Ag NPs could bind the DNA phage, we mixed complementary and non-complementary nanoparticles with the DNA coated viruses. As shown in Figure 1b and Figure S11a, Supporting Information, when the Au@Ag NPs were modified with DNA that is complementary to that on the DNA-phage, we saw almost complete coverage of the phage with nanoparticles. In contrast, when the DNA-Au@Ag NPs were reacted with aldehyde conjugated phage (Figure 1c and Figure S11b, Supporting Information) or when DNA phage were reacted with non-complementary Au@Ag NPs (Figure S11c, Supporting Information) no nanoparticles were bound to any of the viruses. In addition, only when DNA-phage were mixed with complementary DNA-Au@Ag NPs was aggregation seen in solution (Figure S12a, Supporting Information) while the non-complementary and aldehyde phage systems showed none. This was quantitatively also confirmed through UV Vis measurements where only the DNA-phage and complementary DNA Au@Ag NPs showed a dramatic decrease in absorbance due to the Au@Ag NP aggregating out of solution (Figure S12b, Supporting Information). Furthermore, because DNA hybridization was used to couple the SERS nanoparticles to the phage, we tested to see if the number of SERS probes per phage could be increased simply by adding in a second layer of DNA-Cy3-Au@Ag NPs ("DNA2-Cy3-Au@Ag NPs") that were complementary to the first set of DNA-Cy3-Au@Ag NPs ("DNA1-Cy3-Au@Ag NPs") (Figures S13,S14, Supporting Information). TEM analysis qualitatively showed this to be possible which was later confirmed by Raman measurements.

While SERS has been used for biosensing, increasing the number of SERS reporters bound to a single detection agent (antibody, aptamer, phage) in a label-specific manner have not been previously shown. Due to its high surface area and ability to bind multiple SERS particles in response to 1–2 antigens, it was envisioned that the M13 virus would produce much higher SERS intensities as opposed to antibodies, for example. To investigate this possibility, we developed the following assay outlined in **Scheme 1**. First, varying amounts of the model antigen, biotinylated antigoat rabbit IgG were captured to 1 μm streptavidin-coated silica beads. Antigen-bound silica microparticles were then blocked with BSA followed by addition of DNA-conjugated phage. Unbound phage were removed by centrifuge washing the beads three times with buffer. DNA1-Cy3-Au@Ag nanoparticles were next added to the silica bead pellets and vortexed to hybridize with the DNA-phage in sodium citrate buffer. Unbound DNA1-Cy3-Au@Ag NPs were thoroughly removed by stringent washing with buffer followed by filtration through a 0.22 μm filter to remove any possible NP aggregates that would lead to false positives. To generate even higher SERS signal, DNA2-Cy3-Au@Ag NPs were added next to hybridize to the first layer of bound Au@Ag NPs, followed by washing and filtration. The washed and diluted bead solutions were then dried onto Si substrates and individual beads were analyzed by Raman spectroscopy. Since the silica bead showed only a weak Raman peak around 2050 cm^{-1}, this could be easily resolved from the 1580 cm^{-1} fingerprint peak region of Cy3. The assays were run under the same conditions as used previously to determine the EF values for the DNA-Cy3-Au@Ag NPs (power: 130 μW, accumulation time: 30 s, 543.5 nm HeNe laser). As shown in **Figure 2**, with increasing antigen, a distinct increase in Raman intensity was observed with the addition of the first set of SERS particles (DNA1-Cy3-Au@Ag NPs) while the control sample (no antigen) showed virtually no signal. Furthermore, with the second addition of the DNA2-Cy3-Au@Ag NPs, there was a significant enhancement in Raman signal at all antigen concentrations with exponential increases at higher antigen levels. A hypothesis for the exponential increase in signal is that at low antigen concentrations the phage would lie

© 2013 WILEY-VCH Verlag GmbH & Co. KGaA, Weinheim

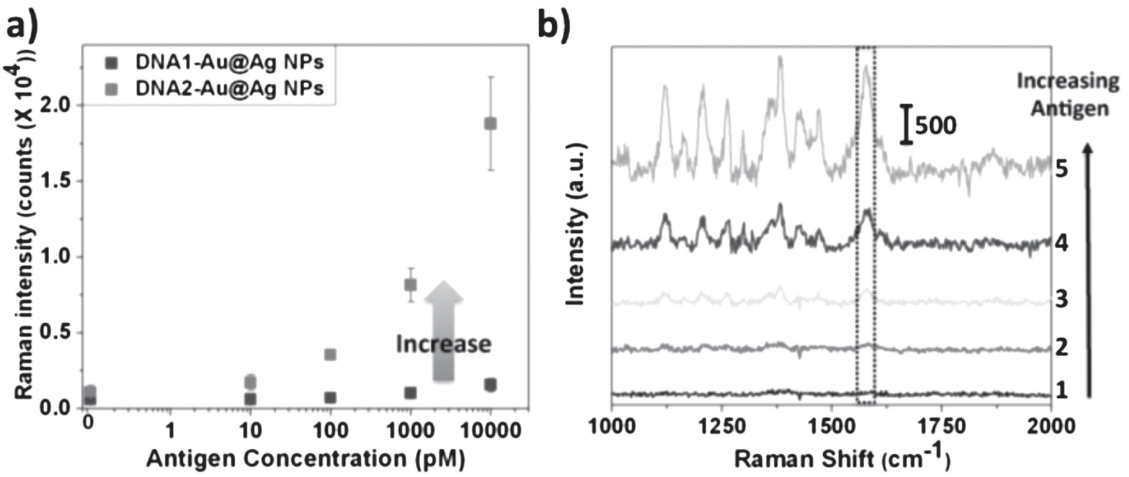

Figure 2. a) Plot of SERS intensities at 1580 cm^{-1} (fingerprint peak of Cy3) as a function of antigen concentration. Each data point represents the sum of Raman intensities measured from nine individual silicon microbeads. Black dots (DNA1-Au@Ag NPs) represent Raman intensities measured after conjugation with DNA1-Au@Ag NPs. Gray dots represent intensities measured after the addition of DNA2-Au@Ag NPs. The error bars represent standard deviations obtained from three separate sensing assays. b) Representative SERS spectra obtained with varying amounts of antigen after conjugation with DNA2-Au@Ag nanoparticles (1: control (no antigen), 2: 10 pM (5 fmol), 3: 100 pM (50 fmol), 4: 1 nM (500 fmol), 5: 10 nM (5 pmol)). Dotted box indicates the fingerprint peak (1580 cm^{-1}) of Cy3.

more parallel to the silica bead surface, while at higher antigen concentrations with larger amounts of phage bound, the filamentous viruses would have greater surface area exposed to bind to the SERS active nanoparticles (Figure S15, Supporting Information), leading to amplified gains in signal. By using this approach, a 2–12 fold enhancement in Raman was obtained with the DNA2-Cy3-Au@Ag NPs than what could be achieved with just DNA1-Cy3-Au@Ag NPs, and concentrations as low as 5 fmol (10 pM) could be easily detected above background (Figure 2).

Since it was hypothesized that the high surface area of each M13 virus (1 μm × 6 nm) was critical for seeing enhanced SERS signals, as a direct comparison we decided to run the exact same protein assay but with DNA conjugated antibodies. For this, using the same hydrazone chemistry and DNA strands as was used to produce DNA conjugated phage, DNA-conjugated goat IgG was synthesized. First, to determine if chemical modification of the antibody could inhibit its ability to bind its protein target, FITC-labeled DNA-conjugated goat IgG was tested for binding to antigoat IgG by fluorescence microscopy. As shown in Figure S16, Supporting Information, chemical modification of the goat IgG did not inhibit it from binding antigoat IgG. Next, using the same working concentrations as those used in the phage assay, we reacted the DNA-conjugated goat IgG with different amounts of its antigen antigoat IgG captured onto the silica microbeads. After removing unbound DNA conjugated antibody, we reacted the beads with the SERS active DNA1-Cy3-Au@Ag NPs. As with the DNA-phage, we further reacted the beads with DNA2-Cy3-Au@Ag NPs to see if any signals could be further amplified. As shown in **Figure 3**, with the DNA-antibody sensor system, very low SERS signals could be obtained as compared with the DNA-phage platform. In the case of 10 nM of antigen, even after conjugation with both DNA1-Cy3-Au@Ag NPs and DNA2-Cy3-Au@Ag NPs, little Raman signal was seen. Through quantitative comparisons, the DNA-phage system was calculated to show nearly a 75-fold increase in Raman intensity over that of the DNA-antibody system (Figure 3). This dramatic increase in SERS signal demonstrates that the high surface area of the filamentous bacteriophage provides significant advantages in terms of sensitivity over that of other systems, such as antibodies. The large differences in SERS signal between the DNA-phage and that of DNA-antibody provides the possibility of running single microbead analysis for multiplexed protein analysis.

3. Conclusion

We have demonstrated here a novel phage-SERS sensing platform as a highly sensitive, facile, and rapid antigen detection system. As a first step, DNA-conjugated metal core–shell nanoparticles were successfully synthesized containing high loadings of Raman active dye. These SERS-active particles were then used in conjunction with DNA-conjugated M13 bacteriophage to yield protein sensing platforms with sensitive Raman detection limits. Additional layers of SERS nanoparticles were also deposited on a single phage via a layer-by-layer approach, leading to exponential gains in Raman intensities. These favorable sensitivities could not be achieved when using antibodies, indicating that the large surface area of bacteriophage provide a mode for enhanced detection over that of existing and conventional biosensing systems. While it was difficult to obtain more than two successive layers of nanoparticles on the phage, by tuning the number of DNA strands per particle and using non-competitive DNA sequences for nanoparticle layering, it should be possible to increase the sensitivity of these phage sensors further. Finally, since each SERS particle may contain a specific dye, and phage may be loaded with specific DNA sequences, it will be possible to extend this for multiplexed analysis in future studies.

© 2013 WILEY-VCH Verlag GmbH & Co. KGaA, Weinheim

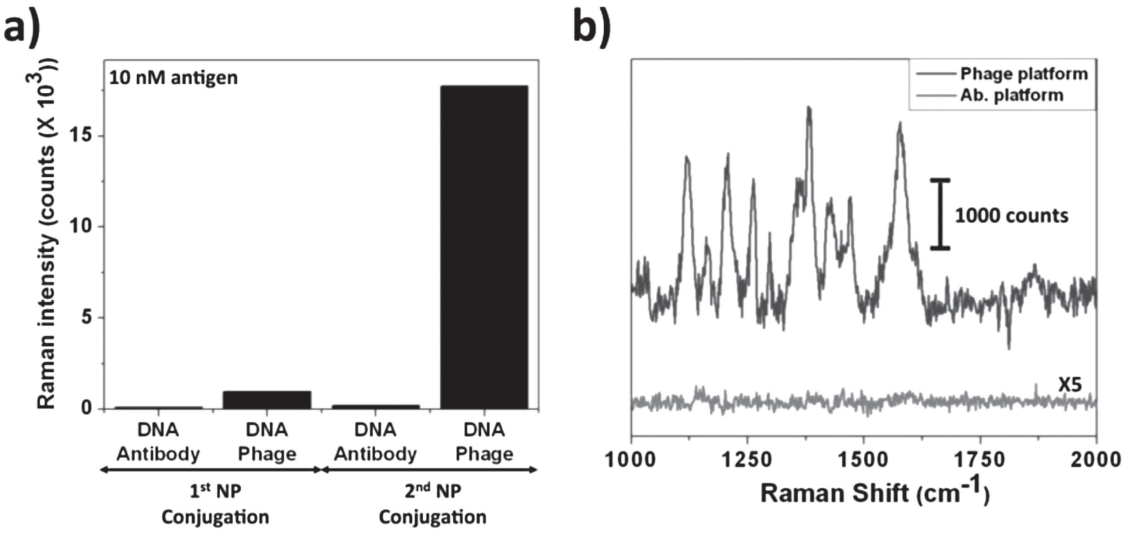

Figure 3. a) Raman intensities obtained from DNA-antibody versus DNA-phage after reacting with DNA1-Cy3-Au@Ag NPs and DNA2-Cy3-Au@Ag NPs. The intensity values were obtained at 1580 cm^{-1} (fingerprint peak of Cy3). Each data point represents the sum of Raman intensities measured from nine individual silicon microbeads. The Raman intensity values were calibrated by subtracting the background signals of no antigen. b) Representative SERS spectra. Comparison plot of Raman spectra obtained between the DNA-phage system and the DNA-antibody sensing system after conjugation with DNA2-Cy3-Au@Ag nanoparticles. In both cases, 10 nM of model antigen was used.

4. Experimental Section

Unless otherwise noted, all reagents were obtained from commercial sources and used without further purification. Water used in buffers or in reactions was deionized with a Milli-Q Advantage A-10 water purification system (MilliPore, USA). UV-vis spectra were acquired on a DU 730 spectrophotometer (Beckman Coulter, USA).

DNA Sequences: All DNA was purchased from Integrated DNA Technology (Iowa, USA).

(1) DNA-phage: 5′-I linker–TTTTTGTGCGCAAAGAGTTT -3′
(2) 1st DNA-Cy3-Au@Ag nanoparticles: 5′-C6-Thiol-AAAAAAAAAA-PEG_{18}-AAACTCTTTGCGCAC -3′′
(3) Capping DNA for DNA-Cy3 Au@Ag nanoparticle: 5′ C6-Thiol-TTTTTTTTT-3′
(4) 2nd DNA-Cy3-Au@Ag nanoparticles: 5′-C6-Thiol-AAAAAAAAAA-PEG_{18}–GTGCGCAAAGAGTTT-3′

Synthesis, Purification, and Characterization of Thiolated Cy3: Sulfo-N-hydroxysuccinimide Cy3 (s-NHS Cy3, 500 mg) (GE Healthcare, USA) was dissolved in DMSO (200 µL) and a solution of cysteamine hydrochloride (6.52 mmol) in pH 8.1 50 mM $NaHCO_3$ buffer (130 µL) was added. The reaction was allowed to proceed overnight at room temperature, at which point the crude reaction mixture was purified by preparatory thin layer chromatography plate (prep TLC) with CH_2Cl_2:MeOH (1:1). The pink bands were collected, eluted with a mixture of ethanol:methanol (9:1), and identified by electrospray ionization mass spectrometry (ESI-MS). The observed mass of the product was 726.30 m/z by ESI-MS (expected mass: 727.18) (Figure S3, Supporting Information) (LCQdeca mass spectrometer with electrospray ionization source, Thermo, USA). The final thiolated Cy3 was dissolved in DMSO and stored at 4 °C.

Synthesis of T_{10}-DNA-Cy3 Au@Ag Nanoparticles: 2 mL of 20 nm citrate-coated gold nanoparticles (Ted Pella, USA) was conjugated with 300-fold molar excess of the synthesized thiolated Cy3 (7.23 µL of 274 µM) overnight at room temperature. Concurrently in a separate reaction, 7 nmol of thiolated DNA in phosphate buffer (PB, 170 mM final concentration, pH 8.0) was treated with dithiothreitol (DTT, 50 mM final concentration) for one hour. DTT-treated thiolated DNA was purified by NAP-5 column (GE Healthcare, USA). Thiolated DNA was then conjugated to the Cy3-20 nm gold nanoparticles by sequentially increasing the NaCl concentration up to 300 mM in the presence of sodium dodecyl sulfate (SDS, 0.1%). After 16 h at room temperature, the DNA-Cy3 gold nanoparticles were purified three times by centrifugation. Next, polyvinylpyrrolidone (PVP, 40k, 0.25 % final concentration), (+)-sodium L-ascorbate (15 mM final concentration), and silver nitrate (0.15 mM final concentration) was sequentially added to the DNA-Cy3 conjugated 20 nm gold nanoparticles (0.5 nM final concentration in dd-H_2O). The solution was adjusted to 300 mM NaCl and 10 mM phosphate buffer, and the reaction was allowed to react for 3 hours with stirring. After centrifugation to collect the DNA-Cy3-Au@Ag nanoparticles, thiolated T_{10} was added to passivate the rest of the nanoparticle surface.

Raman Measurements: A home-built micro-Raman system was used for all Raman measurements, based on an Olympus microscope (BX51TRF) with a 50x objective lens (NPlanFL BD, NA 0.8). The signal was spectrally dispersed and detected with a spectrometer with 600 g mm^{-1} grating and LN2-cooled CCD (Princeton Instruments SP2500i). Green (543.5 nm) and red (632.8 nm) HeNe laser lines were used for excitation, with an edge filter (Semrock) for filtering the laser line.

TEM Sampling and Imaging: Carbon-coated copper mesh TEM grids (Electron Microscopy Sciences, Inc., USA) were glow discharged for 40 s at 20 mA to make them hydrophilic. Several microliters of the phage and nanoparticle solutions were then dropped on the grids and allowed to air dry. Transmission electron microscope (TEM) images were acquired on a CM 100 TEM (Phillips, USA). For imaging M13 bacteriophage, uranyl acetate negative staining was used.

DNA-Phage and DNA-Cy3-Au@Ag NPs-Based Protein Detection and Identification Assay: 1 µm streptavidin coated silica micro particles (15 µL of 10 mg mL^{-1}, Bangs Lab. Inc, USA) were reacted with varying amounts of biotinylated anti-goat IgG (model antigen) in 1× PBS containing 0.025% Tween (0.025% PBST). The antibody-conjugated silica microparticles were blocked with blocking buffer (0.025% PBST, 5 mg mL^{-1} of BSA) for 2 h. Blocked antibody-silica micro particles were collected by centrifuge at 2000 *g* and washed three times (0.025% PBST, 1 mg mL^{-1} of BSA). 750 fmol of DNA-phage was then incubated with the silica micro particles (0.1% PBST, 1 mg mL^{-1} of BSA), and after 1 h incubation, the solution was removed and the silica microparticles were washed three times (0.1 % PBST, 1 mg mL^{-1} of BSA). Phage-bound antibody silica micro particles were then conjugated with DNA-Cy3-Au@Ag nanoparticles (10 µL of 10 nM) in 0.025% SSCT (150 mM NaCl,

© 2013 WILEY-VCH Verlag GmbH & Co. KGaA, Weinheim

15 mM citrate, and 0.025% Tween, pH 7.0), and after 45 min, the DNA1-Cy3-Au@Ag NP-bound silica micro particles were centrifuged at 1000 g, and the supernatant was discarded. The centrifugation purification was repeated. The solution of DNA1-Cy3-Au@Ag NPs were filtered using a 0.22 μm filter (polyvinylidene fluoride (PVDF) membrane, Millipore, USA), and washed with 0.025 % SSCT twice. The particles were dispersed in 250 μL 0.025 % SSCT, and 1 μL of the solution was diluted 10-fold and adsorbed to UVO-treated hydrophilic Si substrate for Raman measurement. The remaining solution of DNA1-Cy3-Au@Ag NPs bound micro particles was reacted with complementary DNA2-Cy3-Au@Ag NPs (10 μL of 10 nM) for 45 min. And washing, Raman samples were prepared as described above. Micro Raman measurements were carried out with separated single silica micro particles with 130 μW, 30 s accumulation time.

Supporting Information

Supporting Information is available from the Wiley Online Library or from the author.

Acknowledgements

This work was supported by an NSF Career Award (DMR-1056808), Office of Naval Research (Award Number: N00014-09-01-0258) and the Sloan Foundation. The authors thank Dr. Joanna Atkin and Prof. Markus Raschke for use of their micro-Raman spectroscopy setup. The authors also thank Prof. Andrew Goodwin for help in editing the manuscript.

Received: August 22, 2013
Revised: October 7, 2013
Published online: December 6, 2013

[1] B. Bohunicky, S. A. Mousa, *Nanotechnol. Sci. Appl.* **2011**, *4*, 1–10.
[2] D. Brambilla, B. L. Droumaguet, J. Nicolas, S. H. Hashemi, L. Wu, S. M. Moghimi, P. Couvreur, K. Andrieux, *Nanomedicine* **2011**, *7*, 521–540.
[3] S. F. Shariat, D. S. Scherr, A. Gupta, F. J. Jr. Bianco, P. I. Karakiewicz, I. S. Zeltser, D. B. Samadi, A. Akhavan, *Arch. Esp. Urol.* **2011**, *64*, 681.
[4] G. R. Souza, D. R. Christianson, F. I. Staquicini, M. G. Ozawa, E. Y. Snyder, R. L. Sidman, J. H. Miller, W. Arap, R. Pasqualini, *Proc. Natl. Acad. Sci. U. S. A.* **2006**, *103*, 1215–1220.
[5] C. Mao, A. Liu, B. Cao, *Angew. Chem., Int. Ed.* **2009**, *48*, 6790–6810.
[6] D. N. Krag, G. S. Shukla, G. Shen, S. Pero, T. Ashikaga, S. Fuller, D. L. Weaver, S. Burdette-Radoux, C. Thomas, *Cancer Res.* **2006**, *66*, 7724–7724.
[7] G. P. Smith, V. A. Petrenko, *Chem. Rev.* **1997**, *97*, 391–410.
[8] C. F. Barbas III, D. R. Burton, J. K. Scott, G. J. Silverman, In *Phage Display. A Laboratory Manual*; Cold Spring Harbor Laboratory Press: New York, **2001**; pp 1.1–16.
[9] J. W. Kehoe, B. K. Kay, *Chem. Rev.* **2005**, *105*, 4056–4072.
[10] I. Yacoby, H. Bar, I. Benhar, *Agents Chemother.* **2007**, *51*, 2156–2163.
[11] P. Ngweniform, G. Abbineni, B. Cao, S. Mao, *Small* **2009**, *5*, 1963–1969.
[12] K. Li, Y. Chen, S. Li, H. G. Nguyen, Z. Niu, S. You, C. M. Mello, X. Lu, Q. Wang, *Bioconjugate Chem.* **2010**, *21*, 1369–1377.
[13] Z. M. Carrico, M. E. Farkas, Y. Zhou, S. C. Hsiao, J. D. Marks, H. Chokhawal, D. S. Clark, M. B. Francis, *ACS nano* **2012**, *6*, 6675–6680.
[14] H. Yi, D. Ghosh, M. Ham, J. Qi, P. W. Barone, M. S. Strano, A. M. Belcher, *Nano Lett.* **2012**, *12*, 1176–1183.
[15] E. R. Goldman, M. P. Pazirandeh, J. M. Mauro, K. D. King, J. C. Frey, G. P. Anderson, *J. Mol. Recogn.* **2000**, *13*, 382–387.
[16] V. A. Petrenko, V. J. Vodyanoy, *J. Microbiol. Methods* **2003**, *53*, 253–262.
[17] J. A. Arter, D. K. Taggart, T. M. McIntire, R. M. Penner, G. A. Weiss, *Nano Lett.* **2010**, *10*, 4858–4862.
[18] J. H. Lee, J. N. Cha, *Anal. Chem.* **2011**, *83*, 3516–3519.
[19] J. H. Lee, D. W. Domaille, J. N. Cha, *ACS Nano* **2012**, *6*, 5621–5626.
[20] D. W. Domaille, J. H. Lee, J. N. Cha, *Chem. Commun.* **2013**, *49*, 1759–1761.
[21] I. E. Torthill, *Semin. Cell Dev. Biol.* **2009**, *20*, 55–62.
[22] E. S. Kawasaki, A. Player, *Nanomedicine: Nanotechnol., Biol. Med.* **2005**, *1*, 101–109.
[23] J. Chen, Y. Miao, N. He, X. Wu, S. Li, *Biotechnol. Adv.* **2004**, *22*, 505–518.
[24] N. L. Rosi, C. A. Mirkin, *Chem. Rev.* **2005**, *105*, 1547–1562.
[25] J. Hahm, C. M. Lieber, *Nano Lett.* **2004**, *4*, 51–54.
[26] D. Kim, W. L. Daniel, C. A. Mirkin, *Anal. Chem.* **2009**, *81*, 9183–9187.
[27] I. L. Medintz, A. R. Clapp, H. Mattoussi, E. R. Goldman, B. Fisher, J. M. Mauro, *Nat. Mater.* **2003**, *2*, 630–638.
[28] Y. Cui, Q. Wei, H. Park, C. M. Lieber, *Science* **2001**, *293*, 1289–1292.
[29] F. Xia, X. Zuo, R. Yang, Y. Xiao, D. Kang, A. Vallée-Bélisle, X. Gong, J. D. Yuen, B. B. Y. Hsu, A. J. Heeger, K. W. Plaxco, *Proc. Natl. Acad. Sci. U. S. A.* **2010**, *107*, 10837–10841.
[30] K. Kneipp, Y. Wang, H. Kneipp, L. T. Perelman, I. Itzkan, R. R. Dasari, M. S. Feld, *Phys. Rev. Lett.* **1997**, *78*, 1667–1670.
[31] S. Nie, S. R. Emory, *Science* **1997**, *275*, 1102–1006.
[32] K. Kneipp, H. Kneipp, I. Itzkan, R. R. Dasari, M. S. Feld, *Chem. Rev.* **1999**, *99*, 2957–2975.
[33] Y. C. Cao, R. Jin, C. A. Mirkin, *Science* **2002**, *297*, 1536–1540.
[34] K. Kneipp, H. Kneipp, I. Itzkan, R. R. Dasari, M. S. Feld, *J. Phys.: Condens. Matter* **2002**, *14*, R597-R624.
[35] J. A. Dieringer, R. B. Lettan II, K. A. Scheidt, R. P. Van Duyne, *J. Am. Chem. Soc.* **2007**, *129*, 16249–16256.
[36] M. K. Hossain, Y. Kitahama, G. G. Huang, X. Han, Y. Ozaki, *Anal. Bioanal. Chem.* **2009**, *394*, 1747–1760.
[37] R. Stevenson, A. Ingram, H. Leung, D. C. McMillan, D. Graham, *Analyst* **2009**, *134*, 842–844.
[38] N. Guarrotxena, G. C. Bazan, *Chem. Commun.* **2011**, *47*, 8784–8786.
[39] S. Kasera, F. Biedermann, J. J. Baumberg, O. A. Scherman, S. Mahajan, *Nano Lett.* **2012**, *12*, 5924–5928.
[40] R. J. Stokes, A. Macaskill, P. J. Lundahl, E. Smith, K. Faulds, D. Graham, *Small* **2007**, *3*, 1593–1601.
[41] S. I. Stoeva, J. Lee, J. E. Smith, S. T. Rosen, C. A. Mirkin, *J. Am. Chem. Soc.* **2006**, *128*, 8378–8379.
[42] R. C. Bailey, G. A. Kwong, C. G. Radu, O. N. Witte, J. R. Heath, *J. Am. Chem. Soc.* **2007**, *129*, 1959–1967.
[43] D. Geißler, L. J. Charbonniere, R. F. Ziessel, N. G. Butlin, H. Löhmannsröben, N. Hildebrandt, *Angew. Chem., Int. Ed.* **2010**, *49*, 1396–1401.
[44] D. Lim, K. Jeon, H. M. Kim, J. Nam, Y. D. Suh, *Nat. Mater.* **2010**, *9*, 60–67.
[45] D. Lim, K. Jeon, J. Hwang, H. Kim, S. Kwon, Y. D. Suh, J. Nam, *Nat. Nanotechnol.* **2011**, *6*, 452–460.
[46] J. Lee, J. Nam, K. Jeon, D. Lim, H. Kim, S. Kwon, H. Lee, Y. D. Suh, *ACS Nano* **2012**, *6*, 9574–9584.
[47] Y. Fang, N-H. Seong, D. D. Dlott, *Science* **2008**, *321*, 388–392.
[48] A. Dirksen, P. E. Dawson, *Bioconjugate Chem.* **2008**, *19*, 2543–2548.
[49] S. J. Hurst, A. K. R. Lytton-Jean, C. A. Mirkin, *Anal. Chem.* **2006**, *78*, 8313–8318.
[50] D.-K. Lim, I.-J. Kim, J. M. Nam, *Chem. Commun.* **2008**, *42*, 5312–5314.
[51] J. H. Lee, G.-H. Kim, J.-M. Nam, *J. Am. Chem. Soc.* **2012**, *134*, 5456–5459.
[52] A. D. McFarland, M. A. Young, J. A. Dieringer, R. P. Van Duyne, *J. Phys. Chem. B* **2005**, *109*, 11279–11285.
[53] Z. Zhang, B. Zhao, L. Hu, *J. Solid State Chem.* **1996**, *121*, 105–110.
[54] J. Lee, A. K. R. Lytton-Jean, S. J. Hurst, C. A. Mirkin, *Nano Lett.* **2007**, *7*, 2112–2115.

© 2013 WILEY-VCH Verlag GmbH & Co. KGaA, Weinheim